Applied Catalysis B: Environmental 304 (2022) 120952

Contents lists available at ScienceDirect

Applied Catalysis B: Environmental

journal homepage: www.elsevier.com/locate/apcatb

Effective regulation of surface bridging hydroxyls on TiO_2 for superior photocatalytic activity via ozone treatment

Biyuan Liu [a], Boge Zhang [a], Jian Ji [a], Kai Li [a], Jianping Cao [a,*], Qiuyu Feng [a], Haibao Huang [a,b,**]

[a] School of Environmental Science and Engineering, Sun Yat-sen University, Guangzhou 510006, China
[b] Guangdong Indoor Air Pollution Control Engineering Research Center, Guangzhou 510006, China

ARTICLE INFO

Keywords:
TiO_2
Ozone treatment
Surface modification
Bridging hydroxyls
Photocatalytic oxidation of toluene

ABSTRACT

A gas-solid and postsynthetic modification was proposed to enrich surface bridging hydroxyls (OH_B) on TiO_2 using ozone. It was found that the adsorbed ozone and its decomposition into oxygen atoms on oxygen vacancies would induce water dissociation and form OH_B, narrowing the bandgap and enhancing the photoresponse. The increased OH_B significantly doubled the efficiency of photogenerated charge carriers transfer, thus generating more reactive oxygen species. Additionally, OH_B provided more adsorption sites for toluene, contributing to the excellent activity and stability. The degradation pathways of toluene containing OH addition and hydrogen abstraction were proposed based on in situ DRIFTS results. Ozone treatment was more effective than other reported surface treatments, and presented a universal improvement on both gas-solid and liquid-solid photodegradation. This work provides a facile, effective, and alternative strategy for the targeted regulation of OH_B on TiO_2 under mild conditions and insight into the mechanism underlying the process.

1. Introduction

Photocatalysis has attracted continuous interest since Fujishima and Honda's pioneering work on photoelectrochemistry on TiO_2 in 1972 [1]. Semiconductor photocatalysts have been proved to show great potential in environmental remediation and solar energy conversion [2,3]. Among them, TiO_2 has been most widely studied owing to its earth-abundance, eco-friendly character, nontoxicity, and high stability [4,5]. However, the recombination of photogenerated charge carriers awfully inhibits the generation of reactive oxygen species (ROS), leading to the low quantum efficiency and poor photocatalytic performance of TiO_2. This presents a great challenge to its industrial application [6]. Therefore, numerous strategies have been developed to enhance charge separation, including surface vacancies formation, heteroatoms doping, co-catalysts deposition, junctions fabrication, and morphology control [7]. Nevertheless, these modification strategies still have many drawbacks, such as vacancy-induced surface lattice corrosion, the environmental risk of the doped heteroatoms, partial blockage on porous surface sites, and the growth of particles. Therefore, it is particularly important to develop an effective strategy to enhance charge separation of photocatalysts.

Recent studies found that hydroxyl groups are effective in enhancing the local spatial charge separation for promoting photocatalytic activity. Yu et al. [8] enriched hydroxyl groups on TiO_2 by hydrothermal treatment to boost photocatalytic activity. Yurdakal et al. [9] investigated the influence of alkaline treatment on TiO_2, which obtained a higher density of surface hydroxyl groups and a sevenfold increase of activity. Wu et al. [10] declared that the cooperative H_2O_2 and NaOH treatment can enhance the water dispersibility and promote dye sensitization of TiO_2 due to the increased hydroxyl groups. Gao et al. [11] synthesized TiO_2 by ethanol-controlled method and significantly improved the H_2-evolution rate with adequate hydroxyl groups acting as the active sites. Casanova et al. [12] used HCl solutions to manufacture TiO_2 with considerable surface OH densities, resulting in efficient oxidation of propene. However, these modification methods are difficult to implement on a mass basis due to their complexity and high energy consumption. In addition, their validity is usually limited to a specific reaction system. Actually, two obvious hydroxyl groups, bridging hydroxyls (OH_B) and terminal hydroxyls (OH_T), are universally recognized on the surface of TiO_2 [13,14]. OH_B acts as hole scavenger and is conducive to photogenerated carriers transfer, leading to better photocatalytic performance than OH_T [15,16]. Currently, rigorous synthesis

* Corresponding author.
** Corresponding author at: School of Environmental Science and Engineering, Sun Yat-sen University, Guangzhou 510006, China.
E-mail addresses: caojp3@mail.sysu.edu.cn (J. Cao), huanghb6@sysu.edu.cn (H. Huang).

https://doi.org/10.1016/j.apcatb.2021.120952
Received 12 August 2021; Received in revised form 13 November 2021; Accepted 17 November 2021
Available online 21 November 2021

or complex treatments are required to obtain rich hydroxyls groups. Furthermore, an increase in OH_B is paralleled by the change of structure, crystallinity, porosity, and surface area of the catalysts, which makes it elusive to clarify the mechanism. A technology enabling targeted alteration of OH_B is urgently needed.

UV-ozone technique has already been used in the treatment of material surface with different purposes [17–19]. However, UV lamps cause high temperature and complicate the development and maintenance of the devices. Researchers are seeking individual ozone treatment for better performance, including surface functionalization and structural regulation. Fakhri et al. [20] applied ozone on an encapsulation strategy for various metal-oxide semiconductors. Maspoch [21, 22] developed a controlled, solid-gas, postsynthetic functionalization in ozone for metal-organic frameworks (MOFs) without compromising the crystallinity. Yuan et al. [23] decreased the electrical sheet resistance and tuned the optical transmittance of the graphene films by using etching-free ozone treatment. Simmons et al. [24] investigated the controllable oxidation of carbon nanotubes by ozone in a short time at room temperature. Inspired by these studies, we envisioned ozone for the effective regulation of hydroxyl groups under mild conditions.

Herein we reported a solid-gas phase and postsynthetic modification of TiO_2 using ozone. X-ray photoelectron spectroscopy (XPS), Fourier transform infrared spectroscopy (FTIR), ^1H nuclear magnetic resonance (NMR), and positron annihilation were conducted to study OH_B on modified TiO_2. Ultraviolet-visible diffuse reflectance spectroscopy (UV-Vis DRS), photoluminescence spectroscopy (PL), electrochemical impedance spectroscopy (EIS), linear sweep voltammogram (LSV), and the transient photocurrent response were employed to analyze optical properties and charge transport. The photocatalytic activity of modified TiO_2 was evaluated by the degradation of gaseous toluene, a typical volatile organic compounds (VOCs) pollutant. The general application of ozone was further examined by photocatalytic oxidation of styrene and methylene blue (MB). Electron spin resonance (ESR), toluene temperature-programmed desorption (toluene-TPD), and in situ diffuse reflectance infrared Fourier transform spectroscopy (DRIFTS) were carried out to investigate the reaction mechanism. This work provided a novel way for the facile regulation of surface hydroxyl groups of TiO_2 under mild conditions and looked insight into its mechanism.

2. Experimental

2.1. Ozone treatment of TiO_2

Typically, 100 mg of commercial TiO_2 (P25, Degussa) were dispersed in 4 mL deionized water. The white suspension was treated by ultrasound for 15 min and then uniformly loaded on 4 glass slides, followed by drying in an oven at 60 °C for 60 min. The as-prepared samples were placed in the flat plate photoreactor. A constant stream of O_3/air (50 mL/min, 300 ppm) was passed through the photoreactor for 12 h. After ozone treatment, the photoreactor was blown by nitrogen to remove residual ozone. TiO_2 after ozone treatment was denoted as O-P25. The O-P25 powder was scraped off from the glass slides for various characterizations. The detailed characterization techniques and photoelectrochemical measurements were shown in Supplementary material.

2.2. Activity evaluation

Photocatalytic oxidation of VOCs (toluene and styrene) was carried out over the as-prepared catalysts in the same flat plate photoreactor after ozone treatment and nitrogen purge. A UV lamp (254 nm, 10 W, Comwin, China) was used to irradiate the TiO_2 films from the top of the reactor through a quartz glass window. The total flow rate was controlled at 1 L/min with VOCs concentration of 20 ppm and relative humidity of 50%. The concentrations of VOCs and CO_2 were measured by an on-line gas chromatograph (GC, 9790II, Fuli, China) equipped with two flame ionization detectors (FID). Thereinto, one FID equipped with KB-5 column (30 m, 0.32 mm ID, 5 μm film thickness) was used for VOCs analysis, while the other FID equipped with a GDX-502 column (2 m, 3 mm ID) and a methanizer were applied for CO_2 analysis. The VOCs conversion (C_{VOCs}) was calculated using the following equation:

$$C_{VOCs}\ (\%) = (1 - [VOCs]_{outlet}/[VOCs]_{inlet}) \times 100\%$$

where $[VOCs]_{outlet}$ and $[VOCs]_{inlet}$ depict the VOCs concentration in outlet and inlet of the reactor, respectively.

The photocatalytic degradation of dyes in the liquid phase used the same UV lamp. 100 mg samples were dispersed in 200 mL 20 ppm MB solution. Before irradiation, the suspension was magnetically stirred for 30 min in dark to establish an adsorption-desorption equilibrium. 1.5 mL liquid was taken at a certain time interval during the experiment and filtrated with nylon syringe filters to remove the catalysts. The residual concentration of MB was monitored through a spectrophotometer (UV-2550, Shimadzu, Japan) and used to calculate the degradation efficiency.

3. Results and discussion

3.1. Structural and surface chemical analysis

The crystalline structure of P25 and O-P25 was firstly investigated. According to the powder X-ray diffraction (XRD) measurements (Fig. S1), both two TiO_2 samples possess typical diffraction peaks of P25 (75% anatase and 25% rutile). No obvious difference in peak position, width, or intensity is observed between them. The results of N_2 adsorption-desorption at 77 K and CO_2 adsorption-desorption at 273 K (Table S1) show the almost identical specific surface area and pore structure on both two TiO_2 [25]. The improved hydrophilicity after ozone treatment, evidenced by the lower water contact angle (Fig. S2), might be attributed to the higher content of surface hydroxyl groups [26]. These results reveal that only surface groups are altered, while the crystal structure, crystallinity, as well as porous texture characterizations are maintained after ozone treatment.

XPS was performed to study the surface chemical states and compositions of two TiO_2 samples. Fig. 1a presents the XPS survey spectrum mainly containing Ti, O, and C elements. For the pristine and modified samples, the characteristic state of Ti^{4+} is determined by the binding energy of 458.7 and 464.4 eV for Ti 2p3/2 and Ti 2p1/2 (Fig. 1b), respectively [27]. It is reported that the water dissociation and OH_T formation result in the changes in peaks position or peaks shape of Ti 2p [28–30]. The high similarity of the Ti 2p spectra demonstrates the identical chemical state of Ti atoms and bare variation of OH_T in these two TiO_2 samples. In Fig. 1c, the deconvoluted O 1s spectra are resolved into three peaks at 530.0, 531.3, and 532.1 eV. The first peak at 530.0 eV represents the lattice oxygen species (O_L), while the other two peaks are assigned to the surface oxygen in hydroxyl groups (O_S) [11]. Previous studies [29,30] showed that the binding energy of OH_B and OH_T were about 1.1–1.3 eV and 2.1–2.3 eV above O_L, respectively. Therefore, the peaks at 531.3 and 532.1 eV can be assigned to OH_B and OH_T, respectively. The fraction of OH_B on O-P25 (15.05%) is much higher than that on P25 (5.60%), confirming the increased OH_B after ozone treatment. As for OH_T, its proportion is almost unchanged, coincident with the result of Ti 2p spectra. Ar^+ ion etching (3 nm depth) was further performed to determine the oxygen species at the bulk of O-P25. After etching, the proportion of OH_B drastically reduces from 15.39% to 5.66% (Fig. 1d), which is similar to that on P25 surface (5.60%). It clearly reveals that the ozone treatment only works on the surface of O-P25 and efficiently increases the OH_B.

FTIR spectroscopy has been extensively used to investigate the presence of surface hydroxyl groups. Fig. 2a shows the FTIR spectra of two TiO_2 samples during stepwise temperature from 50 to 300 °C. The bands at 3630 and 3688 cm^{-1} are assigned to the physisorbed and undissociated water molecules on the surface [31]. With the temperature

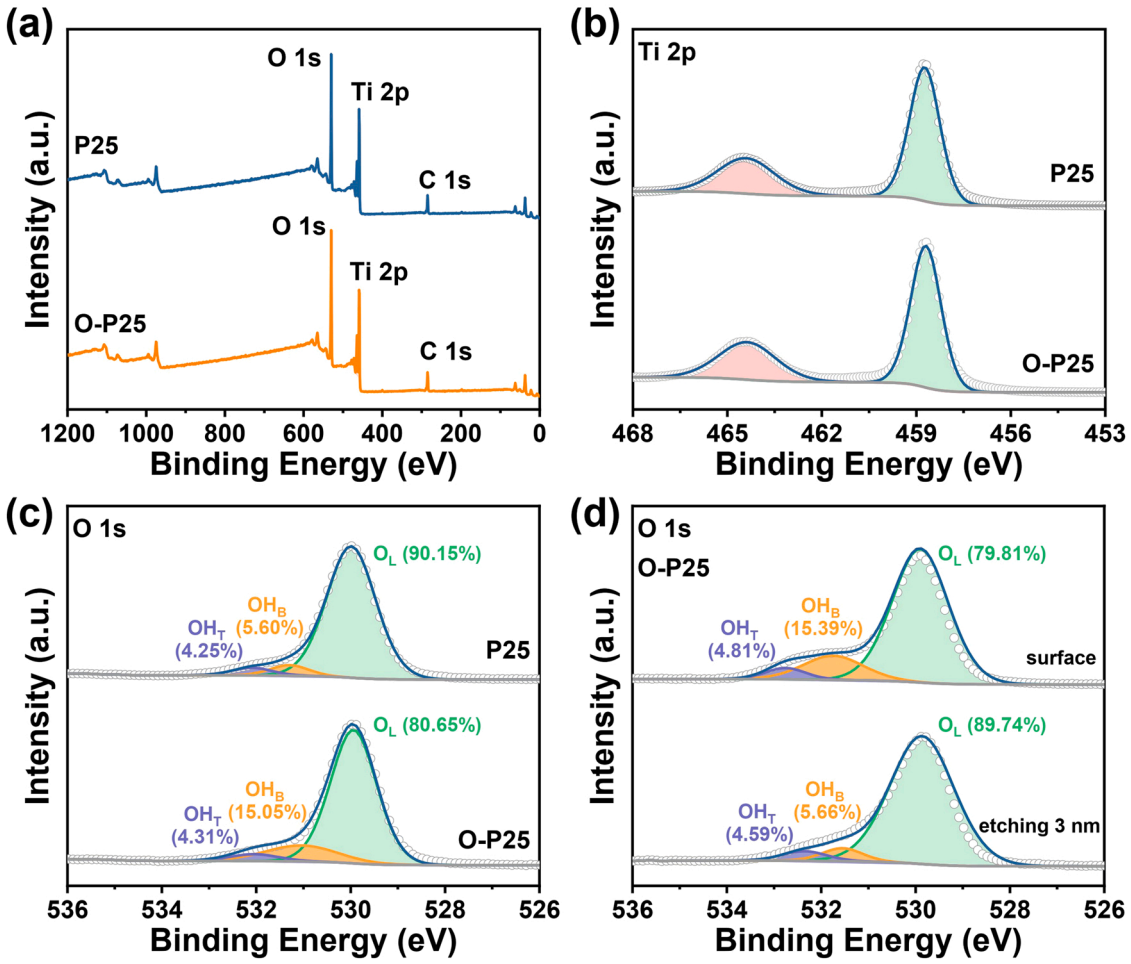

Fig. 1. (a) XPS survey spectrum for P25 and O-P25 samples; XPS spectra in the (b) Ti 2p and (c) O 1s regions; (d) O 1s spectra of O-P25 at surface and 3 nm depth by Ar^+ ion etching. (O_L: the lattice oxygen species, OH_B: the bridging hydroxyls, and OH_T: the terminal hydroxyls).

increasing from 50 to 300 °C, the bands at 3630 and 3688 cm^{-1} almost disappear and new bands at 3649, 3670, and 3711 cm^{-1} appear. These new bands are ascribed to isolated hydroxyl groups. Thereinto, the bands at 3649 and 3670 cm^{-1} are assigned to OH_B, while the band at 3711 cm^{-1} is assigned to OH_T [32]. The stronger absorbance intensity of bands at 3649 and 3670 cm^{-1} in O-P25 indicates that O-P25 has more abundant OH_B than P25.

The changes in hydroxyl groups of TiO_2 after ozone modification were further clarified by ^1H magic-angle spinning (MAS) NMR spectroscopy. As shown in Fig. 2b, an obvious signal with a chemical shift of approximately 6 ppm is observed due to the surface-adsorbed water. The signals at approximately 1.8 and 7.3 ppm can be ascribed to OH_T and OH_B [15,33], respectively. The ratio of OH_B greatly increases from 17.55% on P25 to 28.82% on O-P25. By contrast, the percentage of OH_T changes little from 7.84% to 5.69% after ozone treatment. These results indicate that ozone treatment can effectively enhance OH_B formation on TiO_2 surface.

Different from the powder samples in ^1H MAS NMR and FTIR (electrically neutral), TiO_2 in solution would exchange charge with the bulk solution to form a diffuse electric double layer. To further study the surface properties of the TiO_2 samples, the zeta potential of the TiO_2 suspension in water was measured in a pH range of 3–11. As a result, ozone treatment decreases the isoelectric point from 8.1 to 7.6 (Fig. 2c). It is widely accepted that OH_B is acidic (p*K*a 2.9), whereas OH_T is basic (p*K*a 12.7) [16,34]. The tendency towards the lower isoelectric point of O-P25 indicates that there is more OH_B on its surface.

We further investigated the mechanism of OH_B enhancement on the TiO_2 surface by ozone treatment. Positron annihilation lifetime spectroscopy (PALS) is a sensitive method for studying vacancy-type defects, providing the sizes, types, and relative concentrations of various vacancies [35,36]. Fig. S3 illustrates the positron lifetime spectra of the samples P25 and O-P25, and Table 1 lists the fitting results including two positron lifetime components as well as their relative intensity. The shorter lifetime component (τ_1) is due to vacancy defects, while the longer component (τ_2) is generally caused by the presence of micropore defects. Herein, the relative intensity of τ_1 (I_1) of P25 and O-P25 is 99% and 98%, respectively, which manifests that the main defects are vacancy defects on both pristine and modified samples. The state of surface vacancy defects can be calculated according to the values of $\tau_1{*}I_1$. After ozone treatment, a slight decrease in the values of $\tau_1{*}I_1$ (from 357.30 to 353.45) is observed, revealing the reduction of oxygen vacancies. The fewer oxygen vacancies on O-P25 can be attributed to their filling with ozone and replacement by newly formed OH_B. During the ozone treatment, ozone is preferentially adsorbed on oxygen vacancies, followed by the reaction with the adsorbed water to form six-membered ring species and then transform into OH_B [37]. Some of the ozone would be decomposed into oxygen atoms on vacancies [38,39]. These oxygen atoms further facilitate the water dissociation and the OH_B generation [40–42]. In summary, both ozone and its decomposed products, oxygen atoms, would react with the adsorbed water to form OH_B on oxygen vacancies, leading to the lower amount of vacancies and the higher proportion of OH_B on O-P25.

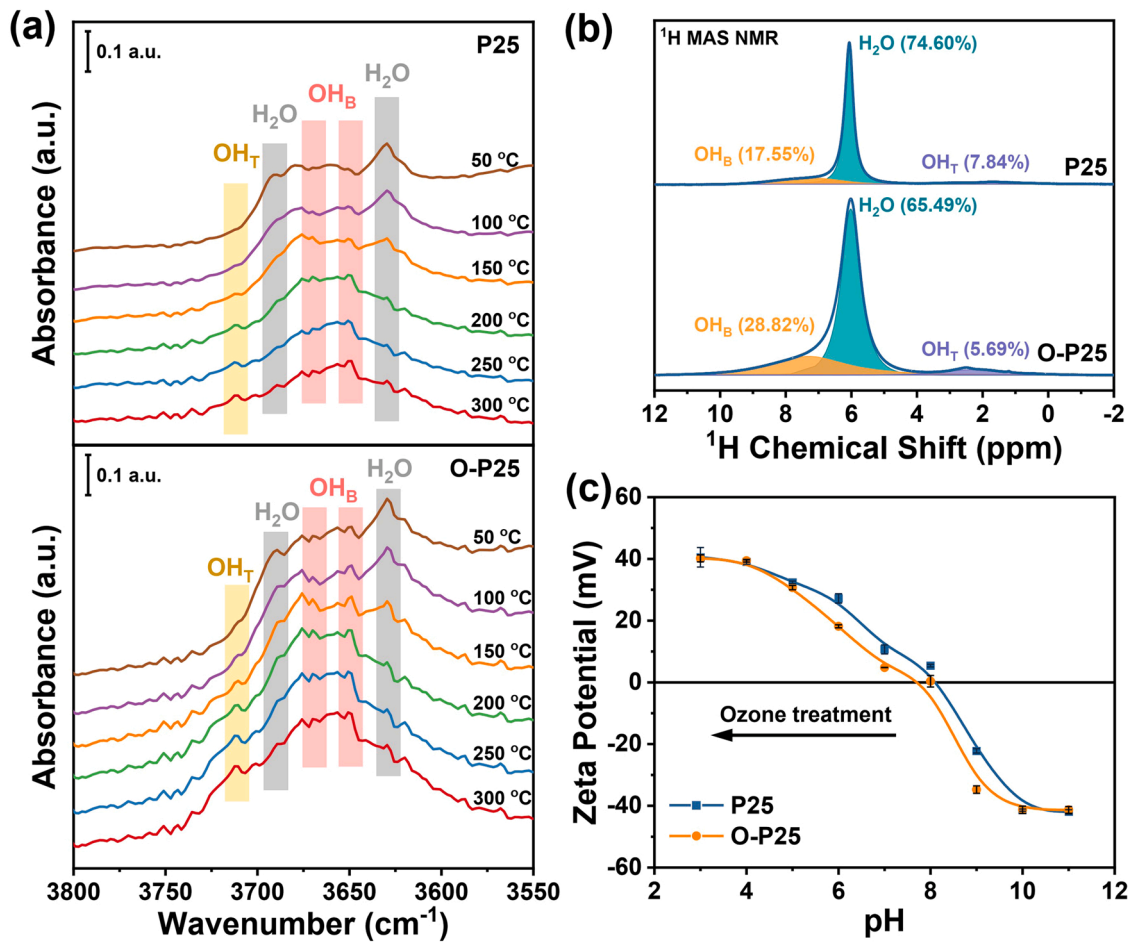

Fig. 2. (a) FTIR spectra in the 3800–3550 cm^{-1} region at different temperatures; (b) ^{1}H MAS NMR spectra; (c) Zeta potential of the P25 and O-P25 samples.

Table 1
The results of positron annihilation experiments: positron lifetime and relative intensity of P25 and O-P25.

Samples		τ_1 (ps)	τ_2 (ps)	I_1 (%)	I_2 (%)	$\tau_1 * I_1$
P25	Value	362.2	1079.1	98.65	1.35	357.30
	Deviation	1.1	104.1	0.27	0.27	–
O-P25	Value	360.8	899.2	97.96	2.04	353.45
	Deviation	1.5	83.1	0.49	0.49	–

τ_1: Positron lifetime of the shorter lifetime component; τ_2: Positron lifetime of the lifetime longer component; I_1: The relative intensity of τ_1; I_2: The relative intensity of τ_2.

3.2. Optical properties and charge transport

So far, we have clearly ascertained that ozone treatment can significantly increase OH_B on the TiO_2 surface. We proceed to explore the impact of increasing OH_B. The photoabsorption plays an important role in the photocatalytic performance, which can be analyzed by UV–vis DRS. In Fig. 3a, both two samples show the strong absorption in the UV region with an absorption edge of approximately 380 nm, on account of the charge transfer from the valence band (VB) O 2p orbital to the conduction band (CB) Ti 3d orbital [43]. A slight red-shift of the absorption edge of O-P25 reveals its outstanding light absorption ability. It is worth noting that the UV-Vis DRS spectra have negligible change after storing at ambient conditions for six months (Fig. S4), indicating high stability of the as-treated samples. The optical absorption and bandgap of semiconductors follow the Kubelka-Munk formula, and the intrinsic bandgap values are shown in Fig. 3b. The O-P25 has a narrower bandgap of 3.23 eV than P25 (3.33 eV) that allows photoexcitation of charge carriers by lower energy photons, conducing to the formation of more photoinduced charge carriers to participate in the photocatalytic reaction. The narrower bandgap can be attributed to the increased amount of OH_B after ozone treatment, which would introduce an excited state and shift the VB to lower energy [44].

Mott-Schottky measurements and VB-XPS were carried out to better understand the energy band structure of P25 and O-P25. From the corresponding Mott-Schottky plots (Fig. 3c), the flat band potential is estimated to be about − 0.49 eV for two TiO_2 samples [45]. Both the samples have positive slope, which declares their typical n-type semiconductor characteristics. In general, the CB potential is 0.1–0.3 eV lower than the flat band potential in the n-type semiconductor [46]. Hence, the CB potential of P25 and O-P25 is determined to be between − 0.59 and − 0.79 eV. The CB potential is more negative than the reduction potential of $O_2/\cdot O^{2-}$ (− 0.33 eV) [47], which identifies that both P25 and O-P25 can generate superoxide anion radicals ($\cdot O_2^-$) from oxygen upon photoirradiation. The formation of $\cdot O_2^-$ can also be proved by the ESR signals in Fig. 5a. The VB-XPS (Fig. 3d) reveals the VB position of P25 (2.67 eV) and O-P25 (2.57 eV). That is, after ozone treatment, the CB depending on Ti 3d states stays the same, while the VB depending on O 2p states shifts to lower energy, consistent with the above UV-Vis results. In summary, the abundant OH_B via ozone treating would shift VB to lower energy, leading to the narrower bandgap and stronger photoresponse.

The separation behavior of photoinduced charge carriers was studied by PL spectra within the range of 320–450 nm at room temperature (Fig. 4a). The P25 displays a strong PL peak at about 375 nm, while the PL peak intensity quenches largely for the O-P25. This result signifies

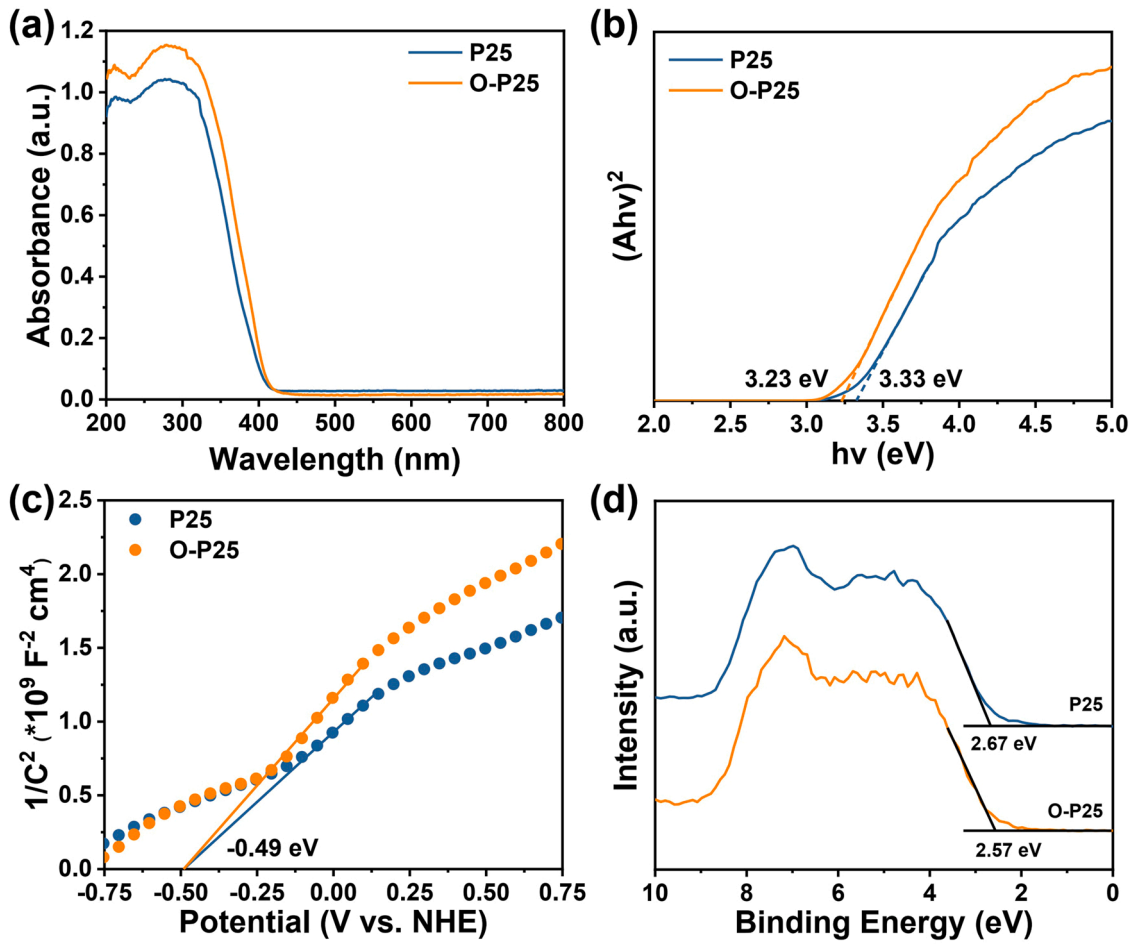

Fig. 3. (a) The UV-Vis DRS spectra and (b) plots of the $(ahv)^2$ vs. photon energy; (c) Mott-Schottky plots at frequencies of 500 Hz; (d) The VB-XPS of the P25 and O-P25 samples.

that O-P25 effectively suppresses the photogenerated carrier recombination, which can be attributed to the increased OH_B after ozone treatment. It is reported [48] that the surface OH groups can preferentially trap photoexcited charge carriers and facilitate charge carrier separation. Photoelectrochemical tests were conducted to explore the efficiency of charge carriers trapping, migration, and transfer. The EIS curves of P25 and O-P25 are displayed in Fig. 4b. Both two materials have smaller charge-transfer resistance (R_{ct}) under UV irradiation than those in the dark, affirming the efficient separation of photoinduced electron-hole pairs and rapid interfacial charge transfer under UV irradiation. Therein, the R_{ct} of O-P25 (7.8 Ω in dark and 2.6 Ω in light) is much smaller than that of P25 (21.8 Ω in dark and 15.3 Ω in light), facilitating the transfer of photogenerated carriers occurring over the electrode surface, which is in good agreement with the PL results. The enhanced charge separation results in higher current density measured from LSV in Fig. 4c. Clearly, the current density of O-P25 is higher than that of P25. Moreover, the twofold response current of O-P25 is observed in light conditions. It can be further confirmed by the transient photocurrent response (Fig. 4d). The photocurrent of P25 and O-P25 instantly increases to a constant value upon the light irradiation and rapidly decreases to the initial stage in the dark, revealing an excellent reproducibility of the tests. The photocurrent of O-P25 remarkably increases to about 15 μA cm^{-2} under light irradiation, twice as much as that of the P25 (approximately 7 μA cm^{-2}), revealing its superior photocarrier generation, separation, and collection efficiencies. In conclusion, the ozone treatment successfully brings about abundant OH_B on the TiO_2 surface, which effectively suppresses photogenerated carrier recombination, boosts charge carrier transfer and rapid separation, and ultimately has a critical influence on the photocatalytic activity.

3.3. The performance and reaction mechanism of photocatalytic toluene degradation

The ROS ($\cdot O_2^-$ and ·OH) production and transformation ability of the samples upon UV irradiation, as an important factor that takes a crucial part in photocatalytic process, were evaluated by recording ESR signals of 5,5-dimethyl-1-pyrroline N-oxide (DMPO)-trapped radicals. The quartet signals of DMPO-·OH (with intensity of 1:2:2:1) and DMPO-$\cdot O_2^-$ (with intensity of 1:1:1:1) were detected over P25 and O-P25 (Fig. 5a). Obviously, the signal strength of ·OH and $\cdot O_2^-$ produced by O-P25 exceeds that of P25 because of the enhanced light utilization and charge separation. It further proves that ozone treatment is an effective way to promote photoinduced charge separation and transfer, as well as the generation of ·OH and $\cdot O_2^-$.

The physical and chemical adsorption behaviors were investigated since they were the first step before the photocatalytic conversion process. The similar specific surface area and pore structure deduce an equivalent capacity of physical adsorption of toluene for both two samples. Toluene-TPD was further utilized to characterize the chemisorption property of toluene on the two samples. With the temperature raised, the desorbed toluene was monitored by an on-line mass spectrometer (MS). As shown in Fig. 5b, the intensity of desorption peaks of O-P25 is higher than that of P25, suggesting that O-P25 is capable of adsorbing more gaseous toluene. This could be beneficial to the subsequent photocatalytic degradation reaction. Additionally, the changes in desorption temperatures confirm the different molecule adsorption

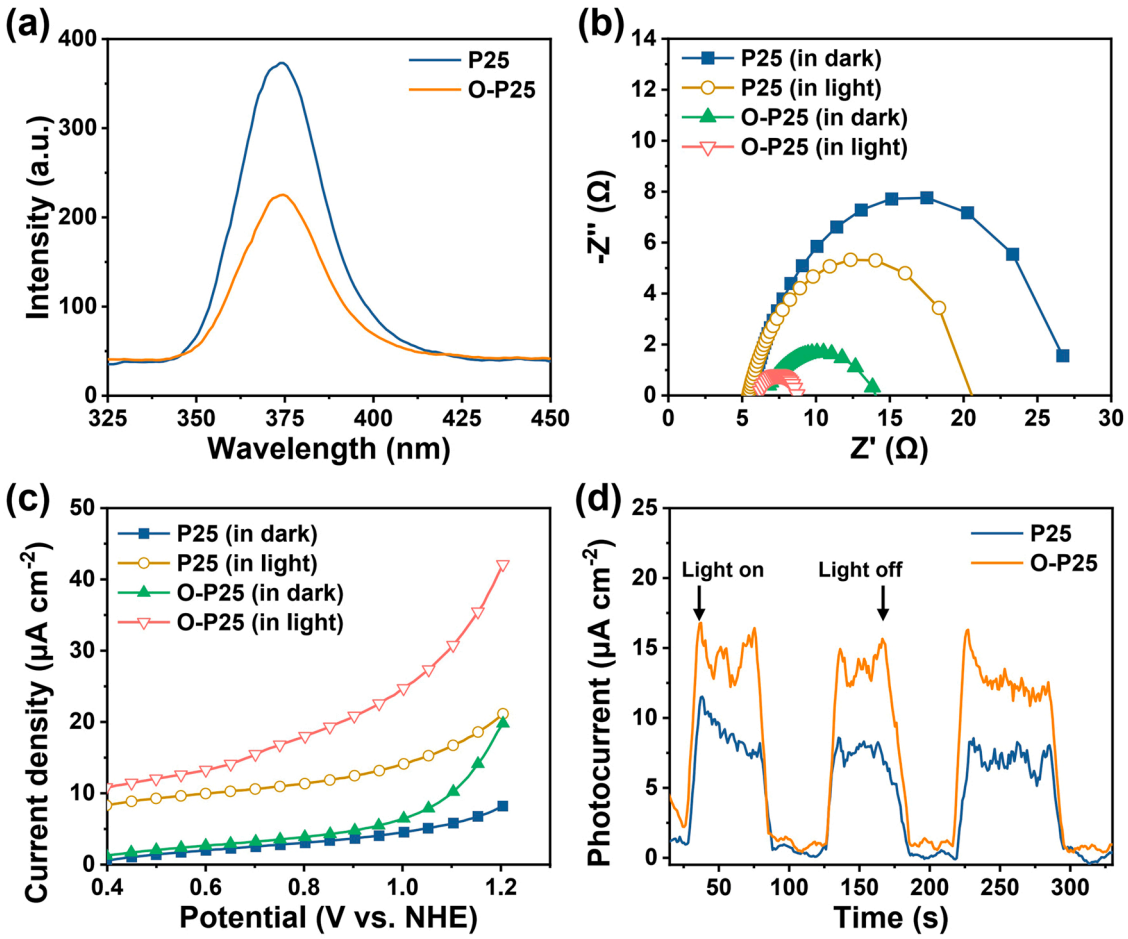

Fig. 4. (a) The PL spectra, (b) EIS curves, (c) LSV profile, and (d) the transient photocurrent response of P25 and O-P25 samples.

configurations on the surface. After Shirley background subtraction and deconvolution, it gives rise to three components at around 90, 220, and 450 °C, corresponding to the weak, moderate, and strong adsorption of toluene on the surface over P25, respectively. The toluene desorption temperatures over O-P25 are higher than those of P25, located at approximately 160, 260, and 540 °C, demonstrating the stronger adsorption of toluene over O-P25. Toluene is proposed to be adsorbed on TiO_2 via OH···π-electron-type interaction, and surface hydroxyl groups on O-P25 acting as active sites for toluene adsorption [49,50]. Specially, the color of O-P25 changed from white to blue, supporting the stronger adsorption of toluene and a higher degree of reduced TiO_2 (Fig. 5c). When temperature rises, toluene may be pyrolyzed to produce CO_2 and reduce the TiO_2 samples, which can explain the darkening of the samples. It is also confirmed by the higher CO_2 signals in Fig. S5a for O-P25. Besides, the H_2O signals detected by the mass spectrometer (Fig. S5b) are assigned to the desorption of hydroxyl groups from the catalyst surface. The desorption temperature of surface hydroxyl groups over O-P25 (ca. 300 °C) is higher than that over P25 (ca. 220 °C). It can verify that O-P25 possesses more OH_B since the OH_B has greater thermodynamic stability and higher desorption temperature than OH_T, which is consistent with the results of FTIR spectra during stepwise temperature [51,52].

Under light irradiation, O-P25 achieves better activity and stability of toluene degradation. As displayed in Fig. 5d, both the toluene conversion and CO_2 concentration over P25 decrease continuously throughout the 120 min reaction, while O-P25 keeps superior performance as the reaction proceeds. The toluene conversion and CO_2 concentration on O-P25 increase by about 10% and 16 ppm, respectively, in comparison with P25 after reaction for 120 min. Furthermore, the O-P25 keeps excellent catalytic stability during toluene degradation. The P25 treated with pure air was tested as a reference sample. It exhibits the same activity as pristine P25 (Fig. S6), assuring the proposed effect of ozone treatment. The activity of P25 modified by other reported surface treatments was also evaluated (Fig. S7). It should be noted that ozone treatment achieves the highest toluene conversion and CO_2 concentration, demonstrating its excellent effectiveness.

In situ DRIFTS was further executed to real-time monitor toluene degradation over the surface of P25 and O-P25. The observed bands and corresponding assignments were summarized in Tables S2 and S3. During the adsorption process of toluene (Fig. 6a), the characteristic bands of toluene appear, indicating the adsorption of toluene on the surface of samples [53–56]. Therein, the weak peaks located at 3028, 2922, and 2872 cm^{-1} are ascribed to the υ(CH) of aromatic ring, while the peak at 2758 cm^{-1} is ascribed to $\upsilon(CH_3)$. The absorption bands at 1603 and 1495 cm^{-1} are typically assigned to the υ(C═C), due to the framework vibration of the aromatic ring. The bands at 1092 and 1120 cm^{-1} are contributed to δ(CH), and bands at 1380 and 1450 cm^{-1} are attributed to symmetric and asymmetric bending modes of the methyl groups. With the toluene adsorption, bands at 3696 cm^{-1} on P25 and 3670 cm^{-1} on O-P25 decrease rapidly, which are assigned to OH_T and OH_B [31], respectively. Meanwhile, two new bands gradually appear, i.e., 3608 cm^{-1} on P25 and 3566 cm^{-1} on O-P25. The new bands are associated with the shift of the hydroxyl bands, revealing that toluene is adsorbed on the catalyst surface via OH···π bond [50]. The stronger intensity of the band at 3566 cm^{-1} demonstrates the stronger adsorption of toluene on O-P25, consistent with the results of the toluene-TPD. Furthermore, a slight absorption peak at 1275 cm^{-1} is observed on O-P25, which can be assigned to the stretching vibration of

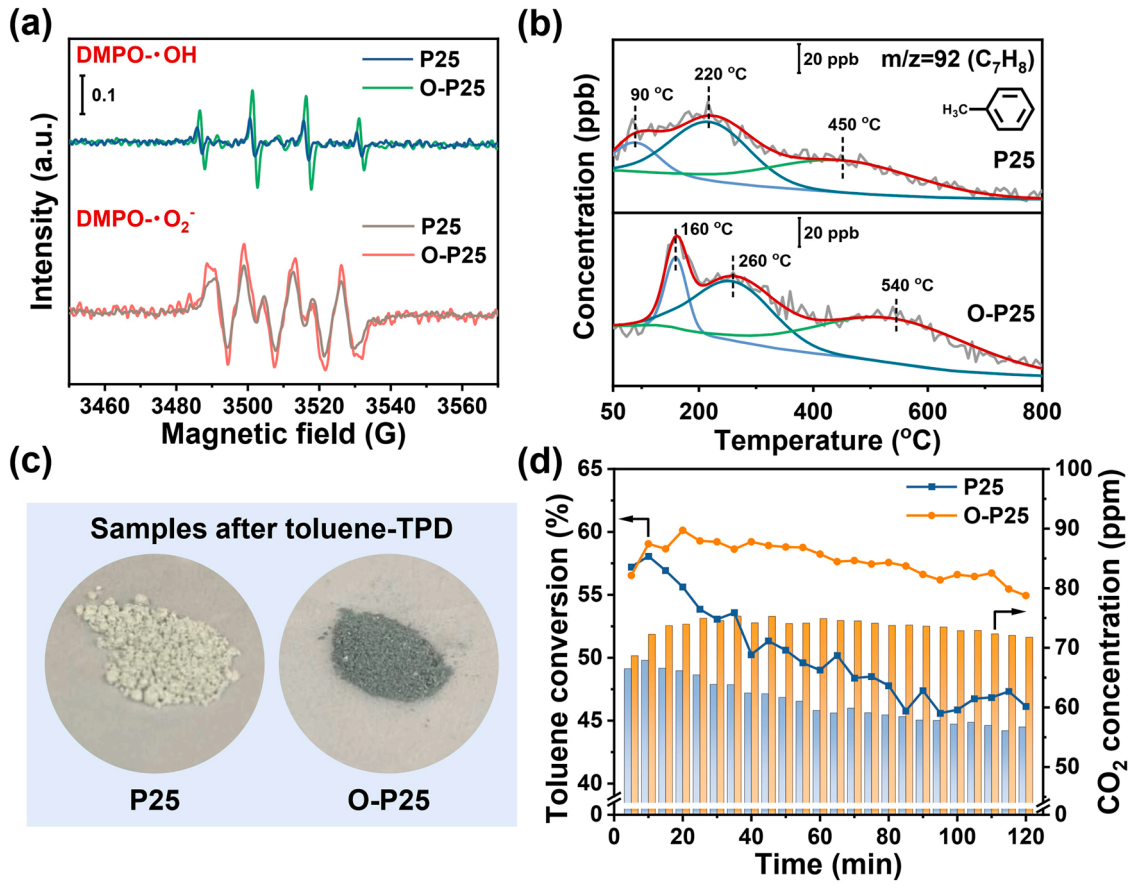

Fig. 5. (a) ESR spectra of DMPO-·O_2^- and DMPO-·OH under UV irradiation; (b) MS signals of toluene-TPD profiles; (c) Digital images after toluene-TPD; (d) Photocatalytic degradation performance of P25 and O-P25 toward gas toluene.

the C-O groups from benzyl alcohol, owing to the pre-oxidation of toluene.

After light irradiation, the intensity of bands assigned to benzyl alcohol (1174 cm^{-1}), benzaldehyde (1220, 1581, and 1645 cm^{-1}), and benzoic acid (1358 and 1415 cm^{-1}) increases rapidly. According to previous studies, benzyl alcohol, benzaldehyde, and benzoic acid are the main intermediate species of toluene oxidation [57–61]. Simultaneously, the bands at 3696 cm^{-1} (OH_T) on P25 and 3670 cm^{-1} (OH_B) on O-P25 decrease drastically in intensity, manifesting that surface hydroxyl groups are consumed in the photocatalytic oxidation of toluene. As Fig. 6b shown, the bands of the intermediate species and surface hydroxyl groups on O-P25 exhibit much larger variations in intensity than those on P25 with the proceeding reaction, revealing that O-P25 consumes more hydroxyl groups to achieve stronger oxidation of toluene.

It was worth noting that a new absorption peak at 870 cm^{-1} appears on O-P25. The peak is regarded as the signal of substituent groups on the aromatic ring such as the vibrational groups of phenolics [61]. Generally, there are two reaction pathways, including different intermediate species for toluene oxidation, i.e., hydrogen abstraction and OH addition [60,61]. Therein, hydrogen abstraction starts with the attack of ·OH on methyl groups and the abstraction of H-atom to form benzyl alcohol, followed by generation of benzaldehyde and then benzoic acid. As for the OH addition process, ·OH attacks the aromatic ring and then replaces the aromatic hydrogen to form cresol. Based on the intermediate species detected by in situ DRIFTS, it can be concluded that hydrogen abstraction is dominant on P25, while both hydrogen abstraction and OH addition are conducted on O-P25 (Fig. 6c). This can be attributed to the generation of more ·O_2^- and ·OH on O-P25. The reaction rate constant for benzyl alcohol, benzaldehyde, and benzoic acid is relatively lower (Table S4). As a result, they are inclined to accumulate on the surface and occupy the active sites, leading to P25 deactivation. Comparably, it is reported that OH addition to the aromatic ring of toluene increases the reaction rate constant for subsequent oxidation via accelerating the path to highly oxidized products [62]. Therefore, the intermediate species are rapidly oxidized and removed from the catalyst surface. It explains the higher toluene degradation activity and stability of O-P25 than P25.

Now, we can descript that the remarkable catalytic behavior of O-P25 is achieved through the following process [63,64]: (i) Large amounts of OH_B promote the adsorption of toluene on O-P25 surface via OH···π-electron-type interaction; (ii) OH_B effectively enhances the surface polarization and drastically facilitates the photogenerated charge carriers separation and transfer to further generate ROS for oxidizing toluene; (iii) The sufficient ROS intensifies the OH addition and accelerates reaction into CO_2 and H_2O; (iv) The consumed surface hydroxyl groups can be continuously supplied by the interaction of water vapor in the gas stream and the catalyst surface. As a summary of the analysis, the increase of OH_B via ozone treatment endows unique and prominent photocatalytic performance. In terms of toluene degradation, it promotes the complete oxidation into CO_2 as well as stability.

3.4. Photocatalytic degradation of other VOCs and dyes

To confirm the general application of the ozone treatment, photocatalytic degradation of styrene gas and MB solution was performed. As presented in Fig. 7a, O-P25 exhibits higher styrene conversion and CO_2 concentration throughout the 120 min reaction. Regarding the degradation of MB solution, O-P25 likewise realizes better activity (Fig. 7b). As mentioned earlier, the increase of OH_B on O-P25 induces the lower shift of the isoelectric point from 8.1 to 7.6 (Fig. 2c). The more negative

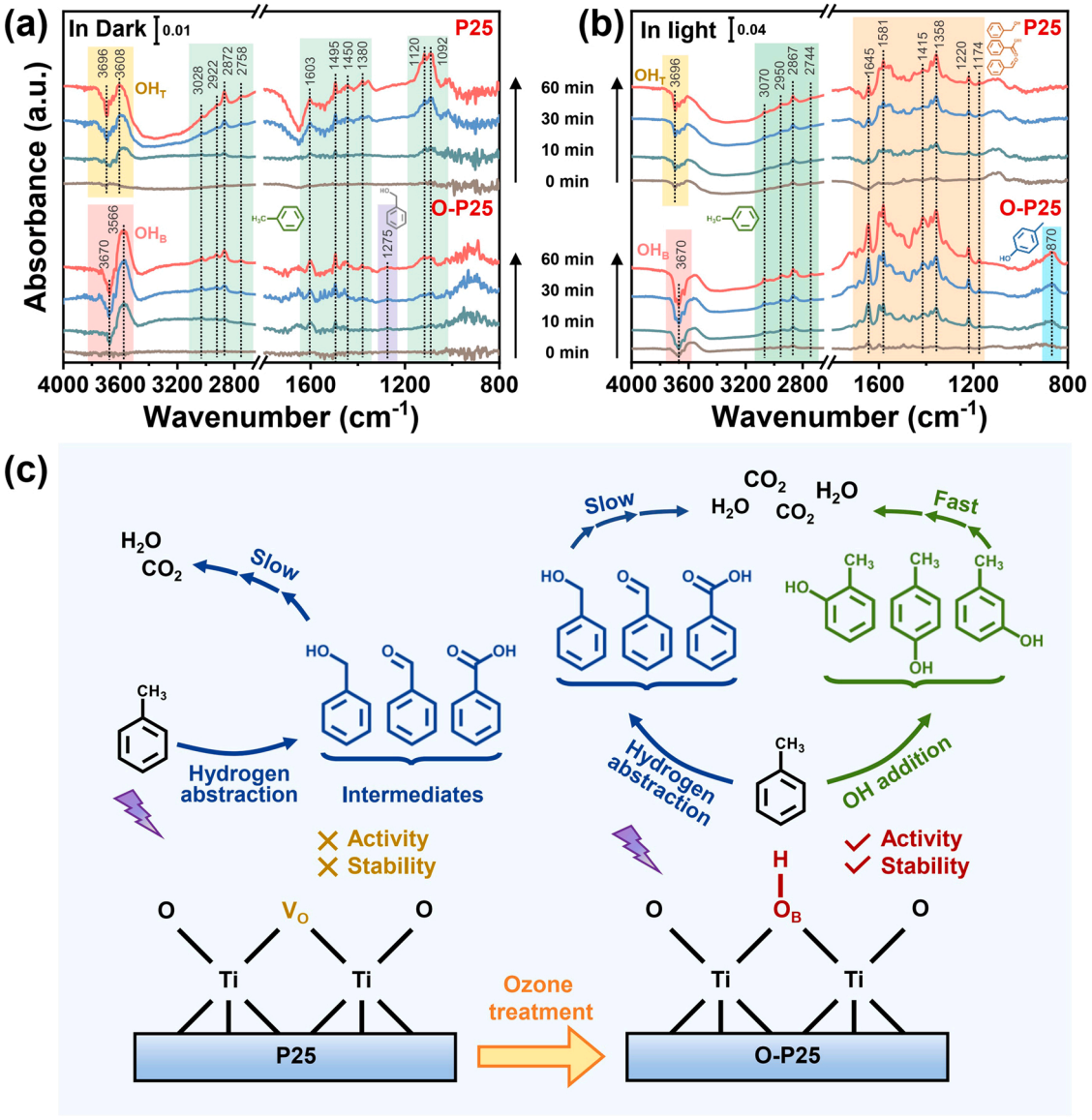

Fig. 6. In situ DRIFTS spectra of (a) the adsorption and (b) the photocatalytic degradation of toluene on P25 and O-P25 samples; (c) Possible reaction mechanism of toluene degradation over the surface of P25 and O-P25.

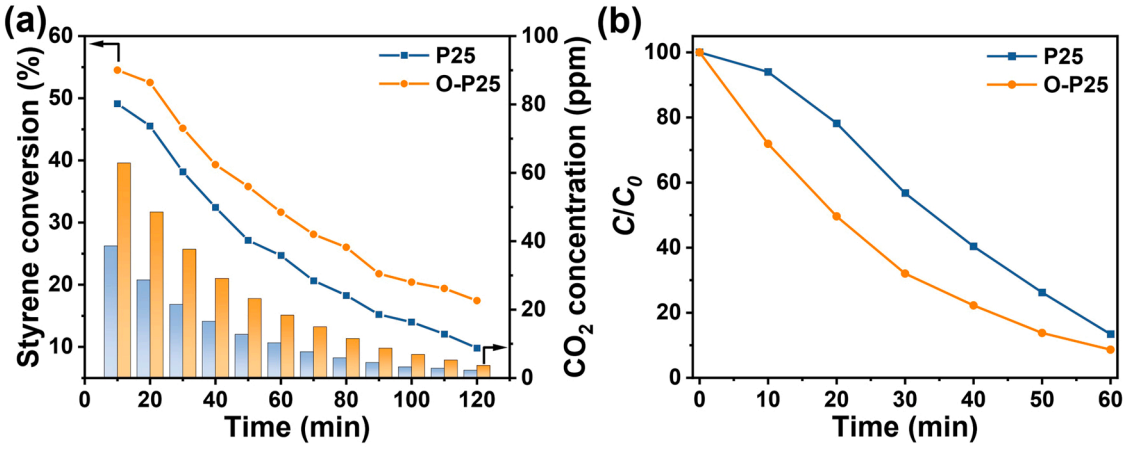

Fig. 7. Photocatalytic degradation performance of P25 and O-P25 toward (a) styrene gas and (b) MB solution.

charges on the TiO_2 surface favor the separation of photogenerated carriers and the generation of ROS. By now, the ozone treatment on TiO_2 has shown a universal improvement in a wide range of heterogeneous photocatalytic reactions, including the gas-solid reaction with different VOCs (toluene and styrene) and liquid-solid reaction with dye (MB solution).

4. Conclusion

In summary, we reported a gas-solid and postsynthetic modification of TiO_2 using ozone. Targeted regulation of OH_B on TiO_2 was achieved by ozone stream at room temperature. Ozone and its decomposition products, atomic oxygen, would induce water dissociation and then form OH_B on the oxygen vacancies. The increase of OH_B narrowed the band gap resulting in the greatly enhanced photoresponse. Also, it significantly doubled the efficiency of photogenerated charge carriers transfer. These contributed to the generation of sufficient reactive oxygen species ($\cdot O_2^-$ and $\cdot OH$), leading to rapid oxidation and removal of intermediate species via OH addition as well as hydrogen abstraction during toluene degradation. Furthermore, the increased OH_B supplied more adsorption sites for toluene. As a result, better activity and stability than other surface treatments were obtained via ozone treatment. Ozone-treated TiO_2 also exhibited universal improvement with better activity in the degradation of styrene gas and MB solution. This study provides a facile strategy to increase the surface hydroxyl groups on TiO_2 catalysts and insight into its mechanism for superior photocatalytic activity.

CRediT authorship contribution statement

Biyuan Liu: Investigation, Visualization, Writing – original draft. **Boge Zhang:** Investigation. **Jian Ji, Kai Li:** Methodology, Writing – review & editing. **Jianping Cao:** Supervision. **Qiuyu Feng:** Formal analysis, Data curation. **Haibao Huang:** Conceptualization, Supervision, Writing – review & editing, Funding acquisition.

Declaration of Competing Interest

The authors declare that they have no known competing financial interests or personal relationships that could have appeared to influence the work reported in this paper.

Acknowledgments

This work was financially supported by the National Natural Science Foundation of China (No. 22076224), Guangdong Basic and Applied Basic Research Foundation (No. 2020A1515010865), Fundamental Research Funds for the Central Universities (No. 20lgjc03), Open Fund of Guangdong Province Engineering Laboratory for Air Pollution Control (No. 2019323609-01) and the Key Laboratory of Water and Air Pollution Control of Guangdong Province (No. 2017A030314001). The authors would like to thank Prof. Zhiquan Chen and Dr. Junjie Liu from Wuhan University for their kind help in positron annihilation experiments.

Appendix A. Supplementary material

Supplementary data associated with this article can be found in the online version at doi:10.1016/j.apcatb.2021.120952.

References

[1] A. Fujishima, K. Honda, Electrochemical photolysis of water at a semiconductor electrode, Nature 238 (1972) 37–38, https://doi.org/10.1038/238037a0.
[2] Y. Boyjoo, H. Sun, J. Liu, V.K. Pareek, S. Wang, A review on photocatalysis for air treatment: from catalyst development to reactor design, Chem. Eng. J. 310 (2017) 537–559, https://doi.org/10.1016/j.cej.2016.06.090.
[3] P. Zhang, X.W.D. Lou, Design of heterostructured hollow photocatalysts for solar-to-chemical energy conversion, Adv. Mater. 31 (2019), 1900281, https://doi.org/10.1002/adma.201900281.
[4] C.H.A. Tsang, K. Li, Y. Zeng, W. Zhao, T. Zhang, Y. Zhan, R. Xie, D.Y.C. Leung, H. Huang, Titanium oxide based photocatalytic materials development and their role of in the air pollutants degradation: overview and forecast, Environ. Int. 125 (2019) 200–228, https://doi.org/10.1016/j.envint.2019.01.015.
[5] Y. Shu, J. Ji, M. Zhou, S. Liang, Q. Xie, S. Li, B. Liu, J. Deng, J. Cao, S. Liu, H. Huang, Selective photocatalytic oxidation of gaseous ammonia at ppb level over Pt and F modified TiO_2, Appl. Catal. B 300 (2022), 120688, https://doi.org/10.1016/j.apcatb.2021.120688.
[6] R. Qian, H. Zong, J. Schneider, G. Zhou, T. Zhao, Y. Li, J. Yang, D.W. Bahnemann, J.H. Pan, Charge carrier trapping, recombination and transfer during TiO_2 photocatalysis: an overview, Catal. Today 335 (2019) 78–90, https://doi.org/10.1016/j.cattod.2018.10.053.
[7] F. Chen, T. Ma, T. Zhang, Y. Zhang, H. Huang, Atomic-level charge separation strategies in semiconductor-based photocatalysts, Adv. Mater. 33 (2021), 2005256, https://doi.org/10.1002/adma.202005256.
[8] J. Yu, H. Yu, B. Cheng, M. Zhou, X. Zhao, Enhanced photocatalytic activity of TiO_2 powder (P25) by hydrothermal treatment, J. Mol. Catal. A: Chem. 253 (2006) 112–118, https://doi.org/10.1016/j.molcata.2006.03.021.
[9] S. Yurdakal, S. Çetinkaya, V. Augugliaro, G. Palmisano, J. Soria, J. Sanz, M. J. Torralvo, S. Livraghi, E. Giamello, C. Garlisi, Alkaline treatment as a means to boost the activity of TiO_2 in selective photocatalytic processes, Catal. Sci. Technol. 10 (2020) 5000–5012, https://doi.org/10.1039/D0CY00755B.
[10] C.Y. Wu, K.J. Tu, J.P. Deng, Y.S. Lo, C.H. Wu, Markedly enhanced surface hydroxyl groups of TiO_2 nanoparticles with superior water-dispersibility for photocatalysis, Materials 10 (2017) 566, https://doi.org/10.3390/ma10050566.
[11] D. Gao, J. Xu, H. Yu, Y. Liu, J. Yu, Hydroxyl-enriched high-crystalline TiO_2 suspensible photocatalyst: facile synthesis and superior H_2-generation activity, Chem. Commun. 57 (2021) 2025–2028, https://doi.org/10.1039/D0CC08277E.
[12] L. Cano-Casanova, A. Amorós-Pérez, M. Ouzzine, M.A. Lillo-Ródenas, M.C. Román-Martínez, One step hydrothermal synthesis of TiO_2 with variable HCl concentration: detailed characterization and photocatalytic activity in propene oxidation, Appl. Catal. B 220 (2018) 645–653, https://doi.org/10.1016/j.apcatb.2017.08.060.
[13] J. Sun, L.H. Guo, H. Zhang, L. Zhao, UV irradiation induced transformation of TiO_2 nanoparticles in water: aggregation and photoreactivity, Environ. Sci. Technol. 48 (2014) 11962–11968, https://doi.org/10.1021/es502360c.
[14] H. Sheng, H. Zhang, W. Song, H. Ji, W. Ma, C. Chen, J. Zhao, Activation of water in titanium dioxide photocatalysis by formation of surface hydrogen bonds: an in situ IR spectroscopy study, Angew. Chem. Int. Ed. 54 (2015) 5905–5909, https://doi.org/10.1002/anie.201412035.
[15] F. Liu, N. Feng, Q. Wang, J. Xu, G. Qi, C. Wang, F. Deng, Transfer channel of photoinduced holes on a TiO_2 surface as revealed by solid-state nuclear magnetic resonance and electron spin resonance spectroscopy, J. Am. Chem. Soc. 139 (2017) 10020–10028, https://doi.org/10.1021/jacs.7b04877.
[16] W. Yu, L. Zhao, F. Chen, H. Zhang, L.H. Guo, Surface bridge hydroxyl-mediated promotion of reactive oxygen species in different particle size TiO_2 suspensions, J. Phys. Chem. Lett. 10 (2019) 3024–3028, https://doi.org/10.1021/acs.jpclett.9b00863.
[17] A. Klasen, P. Baumli, Q. Sheng, E. Johannes, S.A. Bretschneider, I.M. Hermes, V. W. Bergmann, C. Gort, A. Axt, S.A.L. Weber, H. Kim, H.J. Butt, W. Tremel, R. Berger, Removal of surface oxygen vacancies increases conductance through TiO_2 thin films for perovskite solar cells, J. Phys. Chem. C 123 (2019) 13458–13466, https://doi.org/10.1021/acs.jpcc.9b02371.
[18] F. Zhang, B. Hong, W. Zhao, Y. Yang, J. Bao, C. Gao, S. Sun, Ozone modification as an efficient strategy for promoting the photocatalytic effect of TiO_2 for air purification, Chem. Commun. 55 (2019) 3757–3760, https://doi.org/10.1039/C9CC00814D.
[19] T.F. O'Mahony, M.A. Morris, Hydroxylation methods for mesoporous silica and their impact on surface functionalisation, Microporous Mesoporous Mater. 317 (2021), 110989, https://doi.org/10.1016/j.micromeso.2021.110989.
[20] M. Fakhri, N. Babin, A. Behrendt, T. Jakob, P. Gorrn, T. Riedl, Facile encapsulation of oxide based thin film transistors by atomic layer deposition based on ozone, Adv. Mater. 25 (2013) 2821–2825, https://doi.org/10.1002/adma.201300549.
[21] J. Albalad, H. Xu, F. Gandara, M. Haouas, C. Martineau Corcos, R. Mas Balleste, S. A. Barnett, J. Juanhuix, I. Imaz, D. Maspoch, Single-crystal-to-single-crystal postsynthetic modification of a metal-organic framework via ozonolysis, J. Am. Chem. Soc. 140 (2018) 2028–2031, https://doi.org/10.1021/jacs.7b12913.
[22] V. Guillerm, H. Xu, J. Albalad, I. Imaz, D. Maspoch, Postsynthetic selective ligand cleavage by solid-gas phase ozonolysis fuses micropores into mesopores in metal-organic frameworks, J. Am. Chem. Soc. 140 (2018) 15022–15030, https://doi.org/10.1021/jacs.8b09682.
[23] J. Yuan, L.P. Ma, S. Pei, J. Du, Y. Su, W. Ren, H.M. Cheng, Tuning the electrical and optical properties of graphene by ozone treatment for patterning monolithic transparent electrodes, ACS Nano 7 (2013) 4233–4241, https://doi.org/10.1021/nn400682u.
[24] J.M. Simmons, B.M. Nichols, S.E. Baker, M.S. Marcus, O.M. Castellini, C.S. Lee, R. J. Hamers, M.A. Eriksson, Effect of ozone oxidation on single-walled carbon nanotubes, J. Phys. Chem. B 110 (2006) 7113–7118, https://doi.org/10.1021/jp0548422.
[25] N. Bouazza, M.A. Lillo-Ródenas, A. Linares-Solano, Enhancement of the photocatalytic activity of pelletized TiO_2 for the oxidation of propene at low concentration, Appl. Catal. B 77 (2008) 284–293, https://doi.org/10.1016/j.apcatb.2007.07.027.

[26] M. Yu, J. Gong, Y. Zhou, L. Dong, Y. Lin, L. Ma, W. Weng, K. Cheng, H. Wang, Surface hydroxyl groups regulate the osteogenic differentiation of mesenchymal stem cells on titanium and tantalum metals, J. Mater. Chem. B 5 (2017) 3955–3963, https://doi.org/10.1039/C7TB00111H.
[27] D.O. Scanlon, C.W. Dunnill, J. Buckeridge, S.A. Shevlin, A.J. Logsdail, S. M. Woodley, C.R. Catlow, M.J. Powell, R.G. Palgrave, I.P. Parkin, G.W. Watson, T. W. Keal, P. Sherwood, A. Walsh, A.A. Sokol, Band alignment of rutile and anatase TiO_2, Nat. Mater. 12 (2013) 798–801, https://doi.org/10.1038/nmat3697.
[28] S. Benkoula, O. Sublemontier, M. Patanen, C. Nicolas, F. Sirotti, A. Naitabdi, F. Gaie Levrel, E. Antonsson, D. Aureau, F.X. Ouf, S. Wada, A. Etcheberry, K. Ueda, C. Miron, Water adsorption on TiO_2 surfaces probed by soft X-ray spectroscopies: bulk materials vs. isolated nanoparticles, Sci. Rep. 5 (2015) 15088, https://doi.org/10.1038/srep15088.
[29] G. Ketteler, S. Yamamoto, H. Bluhm, K. Andersson, D.E. Starr, D.F. Ogletree, H. Ogasawara, A. Nilsson, M. Salmeron, The nature of water nucleation sites on TiO_2(110) surfaces revealed by ambient pressure X-ray photoelectron spectroscopy, J. Phys. Chem. C 111 (2007) 8278–8282, https://doi.org/10.1021/jp068606i.
[30] P. Krishnan, M. Liu, P.A. Itty, Z. Liu, V. Rheinheimer, M.H. Zhang, P.J. Monteiro, L. E. Yu, Characterization of photocatalytic TiO_2 powder under varied environments using near ambient pressure X-ray photoelectron spectroscopy, Sci. Rep. 7 (2017) 43298, https://doi.org/10.1038/srep43298.
[31] H. Lin, J. Long, Q. Gu, W. Zhang, R. Ruan, Z. Li, X. Wang, In situ IR study of surface hydroxyl species of dehydrated TiO_2: towards understanding pivotal surface processes of TiO_2 photocatalytic oxidation of toluene, Phys. Chem. Chem. Phys. 14 (2012) 9468–9474, https://doi.org/10.1039/C2CP40893G.
[32] A. Mahdavi Shakib, J.M. Arce Ramos, R.N. Austin, T.J. Schwartz, L.C. Grabow, B. G. Frederick, Frequencies and thermal stability of isolated surface hydroxyls on pyrogenic TiO_2 nanoparticles, J. Phys. Chem. C 123 (2019) 24533–24548, https://doi.org/10.1021/acs.jpcc.9b05699.
[33] M. Crocker, R.H.M. Herold, A.E. Wilson, M. Mackay, C.A. Emeis, A. M. Hoogendoorn, ^{1}H NMR spectroscopy of titania. Chemical shift assignments for hydroxy groups in crystalline and amorphous forms of TiO_2, J. Chem. Soc.-Faraday Trans. 92 (1996) 2791–2798, https://doi.org/10.1039/FT9969202791.
[34] H.P. Boehm, Acidic and basic properties of hydroxylated metal oxide surfaces, Discuss. Faraday Soc. 52 (1971) 264–275, https://doi.org/10.1039/DF9715200264.
[35] X. Jiang, Y. Zhang, J. Jiang, Y. Rong, Y. Wang, Y. Wu, C. Pan, Characterization of oxygen vacancy associates within hydrogenated TiO_2: a positron annihilation study, J. Phys. Chem. C 116 (2012) 22619–22624, https://doi.org/10.1021/jp307573c.
[36] Y. Zhao, T. Shi, J. Shang, L. Ding, X. Cao, C. Chen, J. Zhao, Rapid proton exchange between surface bridging hydroxyls and adsorbed molecules on TiO_2, Appl. Catal. B 277 (2020), 119234, https://doi.org/10.1016/j.apcatb.2020.119234.
[37] G. Zhu, J. Zhu, W. Jiang, Z. Zhang, J. Wang, Y. Zhu, Q. Zhang, Surface oxygen vacancy induced α-MnO_2 nanofiber for highly efficient ozone elimination, Appl. Catal. B 209 (2017) 729–737, https://doi.org/10.1016/j.apcatb.2017.02.068.
[38] H. Chen, C.O. Stanier, M.A. Young, V.H. Grassian, A kinetic study of ozone decomposition on illuminated oxide surfaces, J. Phys. Chem. A 115 (2011) 11979–11987, https://doi.org/10.1021/jp208164v.
[39] B. Liu, J. Ji, B. Zhang, W. Huang, Y. Gan, D.Y.C. Leung, H. Huang, Catalytic ozonation of VOCs at low temperature: a comprehensive review, J. Hazard. Mater. 422 (2022), 126847, https://doi.org/10.1016/j.jhazmat.2021.126847.
[40] S. Wendt, R. Schaub, J. Matthiesen, E.K. Vestergaard, E. Wahlström, M. D. Rasmussen, P. Thostrup, L.M. Molina, E. Lægsgaard, I. Stensgaard, B. Hammer, F. Besenbacher, Oxygen vacancies on TiO_2(110) and their interaction with H_2O and O_2: a combined high-resolution STM and DFT study, Surf. Sci. 598 (2005) 226–245, https://doi.org/10.1016/j.susc.2005.08.041.
[41] A.C. Papageorgiou, N.S. Beglitis, C.L. Pang, G. Teobaldi, G. Cabailh, Q. Chen, A. J. Fisher, W.A. Hofer, G. Thornton, Electron traps and their effect on the surface chemistry of TiO_2(110), Proc. Natl. Acad. Sci. USA 107 (2010) 2391–2396, https://doi.org/10.1073/pnas.0911349107.
[42] Z. Zhang, Y. Du, N.G. Petrik, G.A. Kimmel, I. Lyubinetsky, Z. Dohnálek, Water as a catalyst: imaging reactions of O_2 with partially and fully hydroxylated TiO_2(110) surfaces, J. Phys. Chem. C 113 (2009) 1908–1916, https://doi.org/10.1021/jp809001x.
[43] C. Fan, X. Fu, L. Shi, S. Yu, G. Qian, Z. Wang, Disorder modification and photocatalytic activity enhancement of TiO_2 nanocrystals through ultrasonic hydroxylation, J. Alloy. Compd. 703 (2017) 96–102, https://doi.org/10.1016/j.jallcom.2017.01.197.
[44] Y. Zhang, D.T. Payne, C.L. Pang, H.H. Fielding, G. Thornton, Non-band-gap photoexcitation of hydroxylated TiO_2, J. Phys. Chem. Lett. 6 (2015) 3391–3395, https://doi.org/10.1021/acs.jpclett.5b01508.
[45] K. Tang, Z. Wang, W. Zou, H. Guo, Y. Wu, Y. Pu, Q. Tong, H. Wan, X. Gu, L. Dong, J. Rong, Y. Chen, Advantageous role of Ir^0 supported on TiO_2 nanosheets in photocatalytic CO_2 reduction to CH_4: fast electron transfer and rich surface hydroxyl groups, ACS Appl. Mater. Interfaces 13 (2021) 6219–6228, https://doi.org/10.1021/acsami.0c19233.
[46] L. Li, J. Yan, T. Wang, Z.J. Zhao, J. Zhang, J. Gong, N. Guan, Sub-10 nm rutile titanium dioxide nanoparticles for efficient visible-light-driven photocatalytic hydrogen production, Nat. Commun. 6 (2015) 5881, https://doi.org/10.1038/ncomms6881.
[47] X. Ding, H. Liu, J. Chen, M. Wen, G. Li, T. An, H. Zhao, In situ growth of well-aligned Ni-MOF nanosheets on nickel foam for enhanced photocatalytic degradation of typical volatile organic compounds, Nanoscale 12 (2020) 9462–9470, https://doi.org/10.1039/D0NR01027H.
[48] M.A. Henderson, A surface science perspective on TiO_2 photocatalysis, Surf. Sci. Rep. 66 (2011) 185–297, https://doi.org/10.1016/j.surfrep.2011.01.001.
[49] M. Wang, F. Zhang, X. Zhu, Z. Qi, B. Hong, J. Ding, J. Bao, S. Sun, C. Gao, DRIFTS evidence for facet-dependent adsorption of gaseous toluene on TiO_2 with relative photocatalytic properties, Langmuir 31 (2015) 1730–1736, https://doi.org/10.1021/la5047595.
[50] M. Nagao, Y. Suda, Adsorption of benzene, toluene, and chlorobenzene on titanium dioxide, Langmuir 5 (1989) 42–47, https://doi.org/10.1021/la00085a009.
[51] K.S. Finnie, D.J. Cassidy, J.R. Bartlett, J.L. Woolfrey, Ir spectroscopy of surface water and hydroxyl species on nanocrystalline TiO_2 films, Langmuir 17 (2001) 816–820, https://pubs.acs.org/doi/full/10.1021/la0009240.
[52] Y. Murakami, K. Endo, I. Ohta, A.Y. Nosaka, Y. Nosaka, Can OH radicals diffuse from the UV-irradiated photocatalytic TiO_2 surfaces? Laser-induced-fluorescence study, J. Phys. Chem. C 111 (2007) 11339–11346, https://doi.org/10.1021/jp0722049.
[53] A.H. Mamaghani, F. Haghighat, C.S. Lee, Gas phase adsorption of volatile organic compounds onto titanium dioxide photocatalysts, Chem. Eng. J. 337 (2018) 60–73, https://doi.org/10.1016/j.cej.2017.12.082.
[54] G. Mirth, In situ IR spectroscopic study of the surface species during methylation of toluene over HZSM-5, J. Catal. 132 (1991) 244–252, https://doi.org/10.1016/0021-9517(91)90260-B.
[55] A.J. Maira, J.M. Coronado, V. Augugliaro, K.L. Yeung, J.C. Conesa, J. Soria, Fourier transform infrared study of the performance of nanostructured TiO_2 particles for the photocatalytic oxidation of gaseous toluene, J. Catal. 202 (2001) 413–420, https://doi.org/10.1006/jcat.2001.3301.
[56] H. Wang, Xa Dong, W. Cui, J. Li, Y. Sun, Y. Zhou, H. Huang, Y. Zhang, F. Dong, High-surface energy enables efficient and stable photocatalytic toluene degradation via the suppression of intermediate byproducts, Catal. Sci. Technol. 9 (2019) 2952–2959, https://doi.org/10.1039/C9CY00308H.
[57] G. Martra, Lewis acid and base sites at the surface of microcrystalline TiO_2 anatase: relationships between surface morphology and chemical behaviour, Appl. Catal., A 200 (2000) 275–285, https://doi.org/10.1016/S0926-860X(00)00641-4.
[58] R. Méndez Román, N. Cardona Martínez, Relationship between the formation of surface species and catalyst deactivation during the gas-phase photocatalytic oxidation of toluene, Catal. Today 40 (1998) 353–365, https://doi.org/10.1016/S0920-5861(98)00064-9.
[59] P.A. Deveau, F. Arsac, P.X. Thivel, C. Ferronato, F. Delpech, J.M. Chovelon, P. Kaluzny, C. Monnet, Different methods in TiO_2 photodegradation mechanism studies: gaseous and TiO_2-adsorbed phases, J. Hazard. Mater. 144 (2007) 692–697, https://doi.org/10.1016/j.jhazmat.2007.01.097.
[60] B. Liu, Y. Zhan, R. Xie, H. Huang, K. Li, Y. Zeng, R.P. Shrestha, N.T.K. Oanh, E. Winijkul, Efficient photocatalytic oxidation of gaseous toluene in a bubbling reactor of water, Chemosphere 233 (2019) 754–761, https://doi.org/10.1016/j.chemosphere.2019.06.002.
[61] Z. Chen, Y. Peng, J. Chen, C. Wang, H. Yin, H. Wang, C. You, J. Li, Performance and mechanism of photocatalytic toluene degradation and catalyst regeneration by thermal/UV treatment, Environ. Sci. Technol. 54 (2020) 14465–14473, https://doi.org/10.1021/acs.est.0c06048.
[62] R.H. Schwantes, K.A. Schilling, R.C. McVay, H. Lignell, M.M. Coggon, X. Zhang, P. O. Wennberg, J.H. Seinfeld, Formation of highly oxygenated low-volatility products from cresol oxidation, Atmos. Chem. Phys. 17 (2017) 3453–3474, https://doi.org/10.5194/acp-17-3453-2017.
[63] L. Pan, J.J. Zou, X. Zhang, L. Wang, Water-mediated promotion of dye sensitization of TiO_2 under visible light, J. Am. Chem. Soc. 133 (2011) 10000–10002, https://doi.org/10.1021/ja2035927.
[64] L. Pan, J. Zou, X. Liu, X. Liu, S. Wang, X. Zhang, L. Wang, Visible-light-induced photodegradation of rhodamine B over hierarchical TiO_2: effects of storage period and water-mediated adsorption switch, Ind. Eng. Chem. Res. 51 (2012) 12782–12786, https://doi.org/10.1021/ie3019033.